



1,1',2,2'-tetraamino-5,5'-azo-bis-1,3,4-triazole and the electrosynthesis of high-performing insensitive energetic materials

Journal:	<i>Journal of Materials Chemistry A</i>
Manuscript ID	TA-ART-05-2020-005360.R1
Article Type:	Paper
Date Submitted by the Author:	16-Aug-2020
Complete List of Authors:	Yount, Joseph; Purdue University, Materials Engineering Zeller, Matthias; Purdue University System, Department of Chemistry Byrd, Edward; US Army Research Laboratory Weapons and Materials Research Directorate Piercey, Davin; Purdue University, Materials Engineering, Mechanical Engineering

ARTICLE

1,1',2,2'-tetraamino-5,5'-azo-bis-1,3,4-triazole and the electro-synthesis of high-performing insensitive energetic materials

Received 00th January 20xx,
Accepted 00th January 20xx

DOI: 10.1039/x0xx00000x

Joseph R. Yount ^a, Matthias Zeller ^c, Edward F.C. Byrd ^d & Davin G. Piercey ^{*a,b}

Herein, we have demonstrated that electrochemical synthesis of high-performing, insensitive energetic materials in an environmentally friendly manner is possible in a single step from readily available precursors using a synthetic transformation not possible by traditional chemical methods. The electrochemical oxidation of 1,2,5-triamino-1,3,4-triazole in aqueous solution yielded a remarkably stable, high performing new energetic material that was further used to produce various energetic salts. This electrochemically synthesized product and its energetic salts exhibit high thermal stability, low sensitivity towards impact and friction, good calculated detonation performances, and a low-cost synthesis with low toxicity waste streams and amenability to scale up. This work demonstrates electrochemistry's utility towards production of novel modern energetic materials that would otherwise be unobtainable through traditional synthetic pathways.

Introduction

The study of energetic materials, which includes explosives, propellants, and pyrotechnics is a highly practical field of research that endeavors to answer fundamental questions about compounds that lie on the edge of existence. With an important role in both commercial and military applications, the design of novel energetics remains an interesting challenge within modern synthetic chemistry.¹⁻⁶

Traditional energetic materials, such as 2,4,6-trinitrotoluene (TNT) and 1,3,5-trinitro-1,3,5-triazine (RDX), are cost effective, and powerful explosives that utilize the classic method of combining fuel and oxidizer within the same molecule to impart energy content. This method is effective at producing high performing (high detonation velocity and pressure) materials, but the higher performing explosives based on this strategy are often quite sensitive. A current driver in modern energetic materials research is to obtain energetic materials with high performance and stability while additionally minimizing environmental footprint from manufacturing and usage.^{7,8} Complex annulated heterocycles achieve high performances from ring strain, increased packing density from planar

structure, and improvements to heats of formation when based on nitrogen heterocycles.⁹ High nitrogen content materials are of particular interest due to their numerous C-N, and N-N bonds that provide a high heat of formation as a result of the thermodynamic driving force of nitrogenous compounds to decompose forming stable nitrogen gas. High nitrogen energetics often also have lowered environmental impact when compared to traditional energetics; for example aromatic nitro compounds like TNT or cyclic nitramines like RDX are often toxic or carcinogenic, and nitrated compounds in general often produce large amounts of waste acid during synthesis.¹⁰⁻¹³ In addition, synthetic pathways to obtain energetic heterocycle-based materials are still accompanied by numerous steps and often require the use of toxic or heavy metal reactants.^{8,14-16} A viable alternative to produce these materials is electrochemical synthesis.

The use of synthetic electrochemistry is undergoing a "renaissance" of sorts due the unique benefits it offers the synthetic chemist. Numerous resources are available to beginners in the field hoping to incorporate electrochemistry into a traditional a synthetic lab.¹⁷⁻²⁰ Electrochemistry inherently utilizes many of the 12 principles of green chemistry, which can be further applied towards the synthesis of energetics, which helps to mitigate the aforementioned synthetic issues.²¹ The electrons provided from the electrode system act as the primary reagent - which reduces waste streams, reduces or prevents the need for stoichiometric amounts of exogeneous oxidizing/reducing agents, lowers the cost of synthesis, enables unique pathways for energetic synthesis due to electrode polarization, may be performed in recyclable solvents, and provides a high degree of reductive/oxidative control, when compared to

^a Department of Materials Engineering, Purdue Energetics Research Center, Purdue University 205 Gates Road, West Lafayette, IN 47906, USA

^b Department of Mechanical Engineering, Purdue Energetics Research Center, Purdue University 205 Gates Road, West Lafayette, IN 47906, USA

^c Department of Chemistry, Purdue University, 560 Oval Drive West Lafayette, IN 47906

^d Army Research Laboratory, Aberdeen Proving Ground, MD 21005, USA

*Corresponding author email address: dpiercey@purdue.edu

Electronic Supplementary Information (ESI) available: 1. Materials and Methods; 2. X-ray diffraction. See DOI: 10.1039/x0xx00000x

traditional chemical reduction/oxidation.^{22,23} The following examples demonstrate electrochemistry's ability to approach synthesis of energetic materials and precursors. Electrochemical remediation of energetics waste is a highly popular technique, and as Wallace *et al.* had reported, led to the accidental discovery of a novel insensitive high-explosive (IHE) energetic material, azoxytriazolone (AZTO).^{24,25} The electrochemical oxidation of hexanitrobenzyl (HNBB) to produce hexanitrostilbene (HNS) demonstrates a means to eliminate chemical oxidizing species as well as offering potential for scalability.²⁶ The electrochemical synthesis of the energetic precursor potassium 2,2-dinitroethane demonstrated a 90% reduction in waste when compared to the traditional synthetic methodology.²⁷ Numerous studies in recent years have utilized electrochemistry produced annulated triazoles with potential energetic applications via dehydrogenative coupling reactions.²⁸⁻³¹ Additionally, dehydrogenative couplings produce hydrogen gas as a by-product of hydrolysis and hydrogen proton reduction, making them enticing for industrial practices that can utilize this hydrogen as fuel or as a desirable by-product.²¹ Two notable examples from recent literature report direct synthesis of energetic materials electrochemically. Xiaoxue Fu *et al.* recently reported on the formation of well-known energetic azo-tetrazole from readily available 5-aminotetrazole.^{32,33} Baran *et al.* recently published on the formation Cyclobutane at 100 g scale using a flow cell setup.³⁴

Currently, the intentional synthesis of new energetic materials via electrochemistry remains a largely unexplored field. In this work we sought to demonstrate electrochemistry's utility for the synthesis of novel high-nitrogen energetic molecules. Triazoles and azo coupled triazoles are powerful and versatile energetic backbones due to high heats of formation and possess tuneable stability resultant from the incorporation of various functional groups. Their main product of energetic decomposition is environmentally friendly N₂ gas making them a promising alternative to traditional energetic materials. Azo coupling of triazoles not only further improves heat of formation and stability, but azo coupled high nitrogen compounds are notably less toxic when compared to many azobenzene based energetic compounds.³⁵ The precursor for this work, 1,2,5-triamino-1,3,4-triazole [guanazine (**1**)] is a well-known high-nitrogen molecule and is available in a facile one-step synthesis from readily-available precursors hydrazine and dimethylcyanamide, or more conveniently from diaminoguanidine and cyanogen bromide (Figure 1A).^{36,37}

Anodic oxidation of guanazine in water produced the novel energetic molecule 1,1',2,2'-tetraamino-5,5'-azo-bis-1,3,4-triazole [(TAABT) (**2**)] via a suspected oxidative nitrene generation mechanism. We produced five high energy salt derivatives which were chemically characterized by single crystal X-ray diffraction, infrared spectroscopy, multinuclear NMR spectroscopy, elemental analysis, and differential scanning calorimetry (DSC). Experimental investigation of energetic sensitivities towards impact and friction showed these materials to generally be of lower sensitivities than many commonly used energetic materials. Computational calculations using the EXPLO6.05 software package were performed

and show the materials' high energetic performances, being comparable to commonly used military explosive RDX.³⁸

Results and discussion

Examination of compound **1** by cyclic voltammetry (CV), Figure 1(C-D) below, shows three separate oxidation events. An initial reversible one electron oxidation occurs at a peak current (E_{p1}) of 444 mV vs Ag/AgCl followed by two separate one electron irreversible oxidations $E_{p2} = 864$ mV and $E_{p3} = 1456$ mV vs Ag/AgCl. Constant potential electrolysis of guanazine at a cell potential of 2.0 V, under aqueous conditions at room temperature readily produced a red precipitate. Single crystals were produced via diffusion of water into a DMSO solution of the precipitated product in a sealed vial at room temperature. Single crystal X-Ray diffraction revealed the identity of the product formed to be 1,1',2,2'-tetraamino-5,5'-azobis-1,3,4-triazole, **2**, isolated as its monohydrate (**2a**•H₂O and **2b**•H₂O).

Based on the electroanalytical CV studies in Figure 1C-E we propose the reaction pathway shown in Figure 1F. It was hypothesized that this pathway occurs through the formation of a reactive C-nitrene species that undergoes intermolecular insertion to form a hydrazo intermediate, followed by a final oxidation to form the azo complex. It has been shown that electrochemical oxidation is an effective means to access nitrenes.³⁹ Nitrene species are highly reactive and known to undergo a variety of molecular transformations such as nitrene C-H insertions, nitrene cycloadditions, and aryl nitrene ring expansion and contraction.⁴⁰⁻⁴² The ipa/ipc >1 for Figure 1C, indicating that the system was perturbed by a chemical event prior to the reduction of the oxidized species.⁴³ This perturbation was rationalized in Figure 1F as the formation of the azo compound **2**. Additionally, as shown in Figure 1D, E_{p3} decreases from 1456 mV at the initial scan rate of 1000 mV/s to 1129 mV at the final scan rate of 50 mV/s. This decrease in voltage of the peak current was rationalized as a decrease in concentration of guanazine in the solution as a result of forming the dimerized product, which will then lower the potential measured at the electrode according to the Nernst equation.⁴³

Generation of the C-nitrene intermediate rather than the N-nitrene intermediate is believed to be favoured due to radical stabilization from electronic communication with the triazole ring.^{44,45} This is supported by previously-known N-amino compounds having lone pair electrons on the nitrogen that are not in electronic communication with the ring as shown by the N-N bond lengths and free rotation of the of the N-amine vs corresponding C-amines on comparable heterocyclic systems which are in electronic communication.⁴⁴ Therefore, the C-nitrene is stabilized by resonance which would not be possible for the N-amine. This is the proposed reason the azo couple formed at the C-amine, rather than the N-amine where the nitrene species would typically be expected to form. The azo-coupling of a C-amine in the presence of an N-amine is believed to be a unique reaction afforded by this electrochemical synthesis and would be difficult if not impossible to perform via conventional synthetic techniques given the higher reactivity of N-amines towards traditional azo coupling reagents.

For all electrolysis experiments carbon was utilized for the working electrode to prevent alteration to the surface chemistry that may result from Pt or other metals after extended periods of time at high oxidative potentials (i.e., Pt-O formation). Pt was chosen as the cathode due to its fast kinetics for the hydrogen evolution reaction (HER) which will further improve current density.⁴³ Time for the experiments varied depending on current density, but all experiments took approximately 3 hours to reach 2 F/mol electrons passed. When experiments were attempted past 2.5 F/mol the

current density dropped dramatically ($\sim 1\text{mA}/\text{cm}^2$). Due to the low solubility of the dimerized product in aqueous environments, $2\bullet\text{H}_2\text{O}$ readily precipitates and is easily isolated. Neutral pH reaction conditions using 0.1 M LiClO_4 , 0.1M NaNO_3 , or 0.1M triethylammonium acetate resulted in low yields, with a maximum yield of 18.1% (Table 1). Initial studies of variable electrolyte systems revealed insignificant variation in percent yield as a result of the electrolyte used

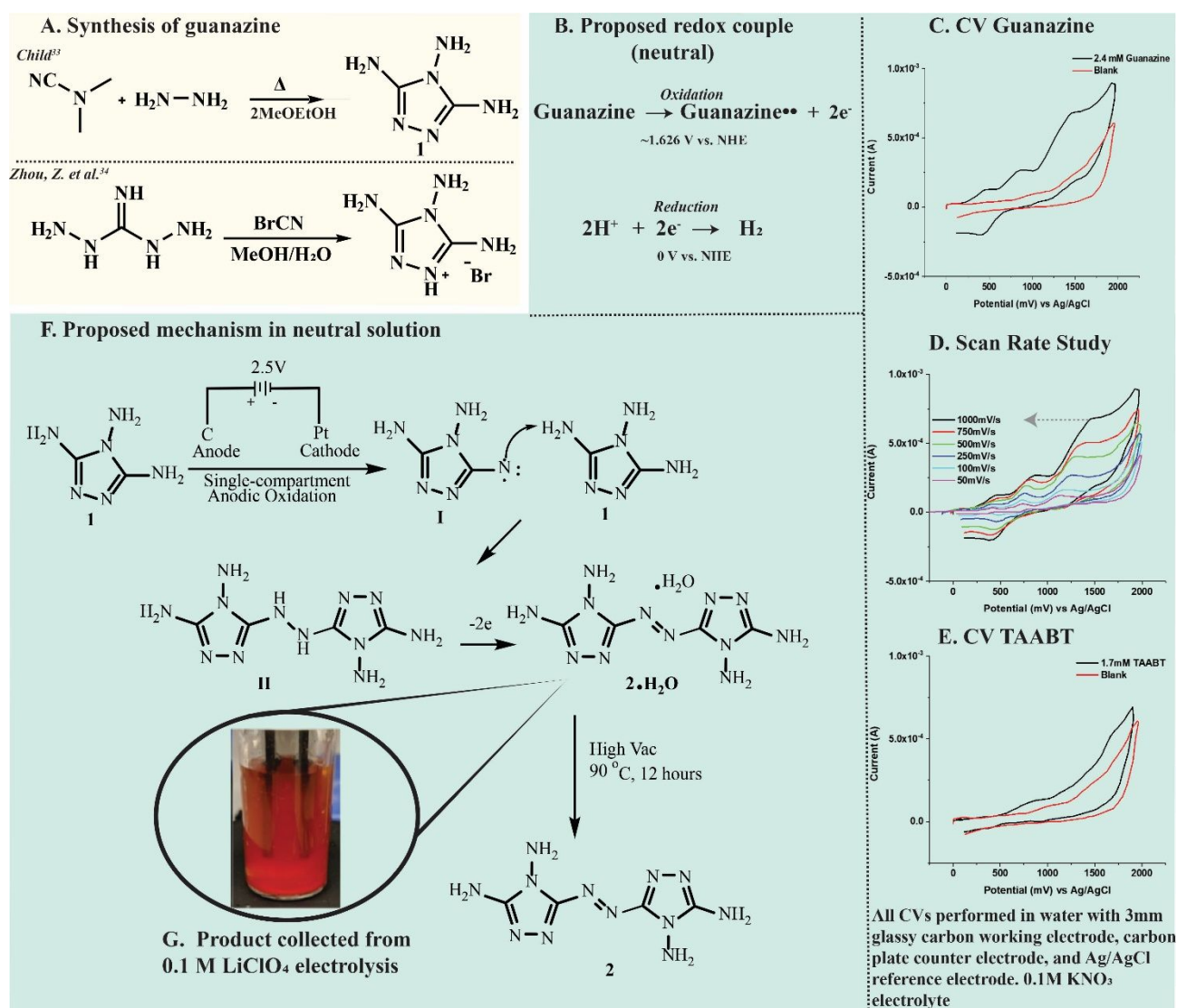


Figure 1: (A) Synthesis of (1). (B) Proposed redox couple for reaction mechanism. (C) CV scans of guanazine in 0.1M KNO_3 and blank electrolyte at 1V/s scan rate. (D) Guanazine variable scan rate study. (E) CVs of 1.7mM TAABT• H_2O and blank electrolyte at 1V/s. (F) Electrochemical synthesis of ($2\bullet\text{H}_2\text{O}$) from (1). (G) Product collected from 0.1 0.1 M LiClO_4 electrolysis.

Further optimization of reaction conditions found that mildly basic electrolytes substantially improve yields. Entries 3 and 4 in Figure 1G show that addition of either 1 or 2 mol eq. of Na_2CO_3 resulted in approximately double the yield over neutral conditions. The highest recorded yield was observed with entry 5 using an ammonium bicarbonate electrolyte. Addition of stronger bases such as NaOH or NH_4OH prevented formation of $2\bullet\text{H}_2\text{O}$ entirely yielding only unidentified decomposition products. Electrolysis under neutral and

acidic conditions followed by quenching with a mild base failed to further precipitate $2\bullet\text{H}_2\text{O}$, indicating that presence of the base may assist in oxidation of guanazine via proton coupled electron transfer. CV studies of guanazine in $(\text{NH}_4)_2\text{CO}_3$, Figure 2A, show the loss of the second oxidation peak and the shift of the third oxidation peak to a lower potential of 1273 mV vs Ag/AgCl which support the idea of a proton coupled electron transfer and has led to the development of the proposed reaction pathway as shown in Figure 2C.³⁰

To test possible overoxidation of $2 \cdot \text{H}_2\text{O}$, a dilute solution of $2 \cdot \text{H}_2\text{O}$ was made and tested by CV as shown in Figure 1E, revealing a lack of oxidation within the potential window of the electrolysis. This suggests that overoxidation of solvated $2 \cdot \text{H}_2\text{O}$ is unlikely. However, overoxidation of initial starting material and formation of unidentified byproducts was observed when the experiments were

conducted at very high potentials (>3.5 V vs H_2O reduction on Pt). Constant current conditions were attempted, however, the potential fluctuated and reached high values from increases in cell resistance due to the large amounts of solid precipitate formed. These experiments also formed unidentified byproducts.

Table 1: Electrolysis results for guanazine using various electrolytes. Potential of 2.5 V vs hydrogen evolution reaction on Pt (entry 1) and 2.5 V vs water reduction on Pt (entries 2-6).

Entry	Electrolyte	Electrodes	Potential (V)	Charge (F mol)	Percent Yield (%)
1	0.1 M $\text{NH}_4\text{Et}_3^+ \text{OAc}^-$	C/Pt	2.5V	2	18.1
2	0.1 M NaNO_3 1mol eq. NaHCO_3	C/Pt	2.5V	2	33.4
3	0.1 M NaNO_3 2mol eq. NaHCO_3	C/Pt	2.5V	2	35.8
4	0.1 M $(\text{NH}_4)_2\text{CO}_3$	C/Pt	2.5V	2	40.2
5	0.1 M NaNO_3 2mol eq. NaOH	C/Pt	2.5V	2	0
6	0.1 M NaNO_3 2mol eq. NH_4OH	C/Pt	2.5V	2	0

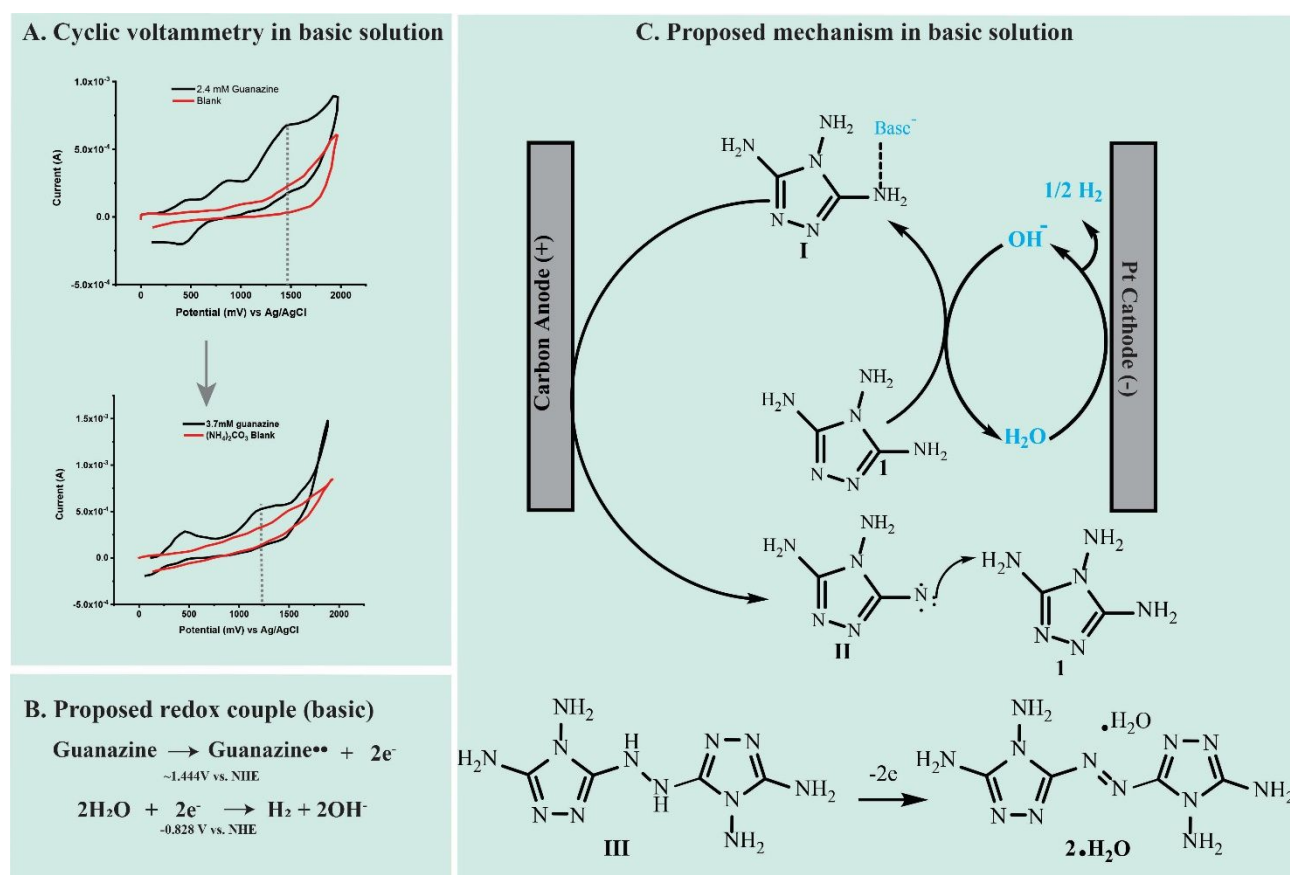


Figure 2: (A) CV of TAABT• H_2O in and blank electrolyte in neutral versus basic solution. This was performed at 1V/s using a 2mm glassy carbon working electrode, carbon plate counter electrode, and Ag/AgCl reference electrode. (B) Proposed redox couple in basic solution. (C) Proposed mechanism for the anodic azo coupling of guanazine to produce TAABT (**2**) in basic solution.

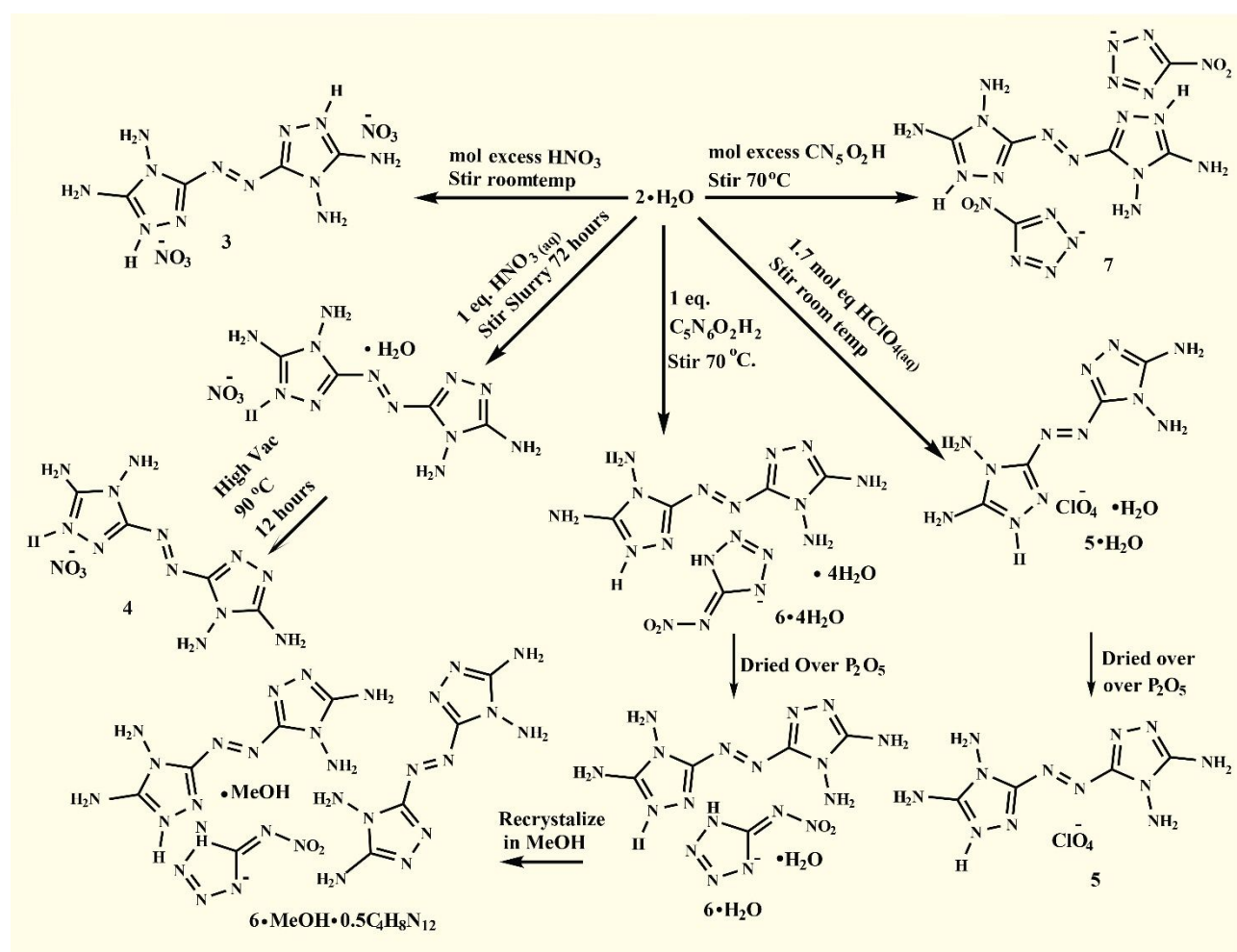
Syntheses of salts

Salts **3-7** were prepared by simple acid-base chemistry by reaction of **2** with nitric acid, perchloric acid, 5-nitrimino-1,2,3,4-tetrazole, or 5-nitro-1,2,3,4-tetrazole in an aqueous solution (Scheme 1). Salt **3** was produced from a molar excess addition of concentrated nitric acid to an aqueous slurry of **2** at room temperature with stirring. After complete dissolution of **2**, the solution was slowly crystallized

yielding light orange plate-like crystals suitable for X-ray measurements. Salt **4** was synthesized by combining an equimolar solution of HNO_3 and **2** in aqueous solution with continuous stirring for 3 days, yielding a light orange slurry. This slurry was filtered and isolated and after crystallization from water yielded crystals suitable for X-ray measurements revealing a monohydrate crystal structure $4 \cdot \text{H}_2\text{O}$. $4 \cdot \text{H}_2\text{O}$ was placed into a round bottom flask and dried under

high vacuum on a Schlenk line at 90 °C for 12 hours yielding a dry powder that that was identified as anhydrous **4** by elemental analysis. Salt **5** was produced similarly to **3**, by addition of a molar excess of HClO₄ to an aqueous slurry of **2** with stirring. Crystallization of the solution yielded orange plate-like crystals that revealed a monohydrate crystal structure by X-ray measurement. Drying of **5**•H₂O over P₂O₅ in a desiccator produced light yellow crystals that were identified as anhydrous **5** by elemental analysis. A crystal structure for **5** was obtained by slow recrystallization from MeOH that yielded fine yellow needle crystals suitable for X-ray measurement. Dissolution of **2** in an aqueous solution of 5-nitrimino-1,2,3,4-tetrazole was only possible in large volumes of water with heating.

Crystallization of **6** yielded fine needle red crystals that were suitable for X-ray measurements and where were identified as a tetrahydrate, **6**•4H₂O. Drying this tetrahydrate over P₂O₅ yielded the monohydrate **6**•H₂O as determined by elemental analysis. Recrystallization from methanol yielded a methanol solvate cocrystal of **6** with unprotonated **2** (**6**•MeOH•0.5C₄N₁₂H₈). Salt **7** was produced similarly to **6**, however; 5-nitro-1,2,3,4-tetrazole is more acidic and more readily protonated than **2** without heating. Recrystallization yielded yellow needles suitable for X-ray measurement. Salts **3** and **7** were the only crystal structures in which the acid doubly protonated TAABT (**2**).



Scheme 1: Syntheses of salts 3-7. (**3**) 1,1',2,2' tetra-amino-5,5'-azo bis-1,3,4-triazolium, (**4**) 1,1',2,2' tetra-amino-5,5'-azo bis-1,3,4-triazolium nitrate, (**5**) 1,1',2,2' tetra-amino-5,5'-azo bis-1,3,4-triazolium perchlorate, (**6**) 1,1',2,2' tetra-amino-5,5'-azo bis-1,3,4-triazolium 5-nitrimino-1,2,3,4-tetrazolate monohydrate, (**7**) 1,1',2,2' tetra-amino-5,5'-azo bis-1,3,4-triazolium di-5-nitro-1,2,3,4-tetrazolate.

Single Crystal X-ray Structure Determinations

Neutral compound **2a** crystallizes in the triclinic, P1 space group with a density of 1.626 g/cm³ at 150 K and 2 symmetry units per cell. This density is notably lower than TAABT polymorph **2b**, which crystallizes in the monoclinic space group P21/c with a density of 1.723 g/cm³ at 150 K and 4 formula units per unit cell. The difference between the polymorphs is the direction the hydrogen atoms point

on the N-amine; in **2a** the hydrogen atoms point inward and in **2b** they point outward. Nitrate salt **3** crystallizes in the triclinic space group P1 with a density of 1.789 g/cm³ at 150 K and 1 formula unit per unit cell. Nitrate salt **4**•H₂O crystallizes in the monoclinic space group P21/n with a density of 1.752 g/cm³ at 150 K and 4 symmetry units per cell. The crystal under investigation for salt **4**•H₂O was

found to be non-merohedrally twinned and further solution data for this crystal can be found in the supplementary information. Perchlorate salt 5 crystallizes in the monoclinic space group $P2_1/c$ with the highest observed density in this work of 1.821 g/cm³ at 150 K and 2 symmetry units per cell. The cation is monocationic (two protons shared between two neighboring cations). The ammonium H atom is located on a twofold axis and is shared between two symmetry equivalent N atoms. Both anion and cation are located on special positions and each half of the ion is within the asymmetric unit. Salt 5•H₂O crystallizes in the monoclinic space group $P2_1/c$ with a density of 1.748 g/cm³ at 150 K and 4 symmetry units per cell. The

structure of 6•4H₂O is metrically orthorhombic but crystallizes in $P2_1/n$ as a pseudomerohedric twin, with close to 1:1 twin ratios (0.521(2):0.479(2)). The density of 6•4H₂O is 1.622 g/cm³ with 4 symmetry units per cell. The lowered density compared to the others is due to the 4 waters of hydration. 6•MeOH•0.5C₄H₈N₁₂ crystallizes in the triclinic space $P\bar{1}$ with a density of 1.669 g/cm³ at 150 K and 2 symmetry units per cell. Nitrotetrazolate salt 7 crystallizes in the monoclinic space group $P2_1/c$ with a density of 1.762 g/cm³ at 150 K and 2 symmetry units per cell.

Table 2. X-ray data and parameters of TAABT and energetic salts.

	2•H ₂ Oa	2•H ₂ O _b	3	4•H ₂ O	5•H ₂ O	5	6•4H ₂ O	6•MeOH •0.5(C ₄ H ₈ N ₁₂)	7
Formula	C ₄ H ₈ N ₁₂ •H ₂ O	C ₄ H ₈ N ₁₂ •H ₂ O	[C ₄ H ₁₀ N ₁₂] ²⁺ [2(NO ₃)] ²⁻	[C ₄ H ₉ N ₁₂] ⁺ [NO ₃] ⁻ •H ₂ O	[C ₄ H ₉ N ₁₂] ⁺ [ClO ₄] ⁻ •H ₂ O	[C ₄ H ₉ N ₁₂] ⁺ [ClO ₄] ⁻	[C ₄ H ₉ N ₁₂] ⁺ [CHN ₆ O ₂] ⁻ •4(H ₂ O)	[C ₄ H ₉ N ₁₂] ⁺ [CHN ₆ O ₂] ⁻ •0.5(C ₄ H ₈ N ₁₂) •CH ₃ O	[C ₄ H ₁₀ N ₁₂] ²⁺ [2(CN ₃ O)] ²⁻
M _r [g mol ⁻¹]	242.24	242.24	350.26	305.26	342.70	324.68	426.37	498.46	454.36
Crystal system	Triclinic	Monoclinic	Triclinic	Monoclinic	Monoclinic	Monoclinic	Monoclinic	Triclinic	Monoclinic
Space Group	$P\bar{1}$	$P2_1/c$	$P\bar{1}$	$P2_1/n$	$P2_1/c$	$P2_1/c$	$P2_1/n$	$P\bar{1}$	$P2_1/c$
Color	Orange	Red	Orange	Orange	Orange	Yellow	Red	Yellow	Orange
Habit	Plate	Rod	Block	Plate	Plate	Needle	Needle	Needle	Needle
Size [mm]	0.45 × 0.25 × 0.18	0.35 × 0.11 × 0.10	0.22 × 0.20 × 0.15	0.33 × 0.28 × 0.11	0.35 × 0.33 × 0.16	- - -	0.55 × 0.05 × 0.03	0.20 × 0.03 × 0.01	0.55 × 0.23 × 0.19
a [Å]	7.968 (5)	11.091 (7)	6.689 (2)	7.308 (3)	7.648 (4)	7.410 (6)	6.901 (4)	8.350 (11)	5.532 (3)
b [Å]	8.142 (5)	12.028 (7)	8.682 (3)	16.635 (7)	18.754 (10)	8.693 (9)	15.047 (8)	10.757 (17)	14.965 (8)
c [Å]	8.418 (6)	7.087 (5)	12.025 (5)	9.625 (4)	9.465 (5)	9.554 (7)	16.811 (10)	12.007 (16)	10.665 (5)
α [°]	89.45 (2)	90	80.34 (17)	90	90	90	90	104.53 (10)	90
β [°]	69.47 (2)	99.01 (3)	75.03 (15)	98.40 (14)	106.36 (16)	105.80 (5)	90.01 (4)	107.05 (9)	856.35 (8)
γ [°]	76.13 (2)	90	77.99 (14)	90	90	90	90	91.66 (1)	90
V [Å ³]	494.9 (6)	933.7 (10)	655.05 (4)	1157.5 (8)	1302.5 (12)	592.2 (9)	1745.7 (17)	992.0 (3)	856.4 (8)
Z	2	4	2	4	4	2	4	2	2
ρ _{calcd} [g cm ⁻³]	1.626	1.723	1.776	1.752	1.748	1.821	1.622	1.669	1.762
μ [mm ⁻¹]	0.13	0.14	0.16	0.15	0.35	3.34	1.24	1.17	0.15
F(000)	252	504	360	632	704	332	888	516	464
T [K]	150	150	150	150	150	150	150	150	150
θ _{min} , θ _{max} [°]	2.6, 33.2	2.5, 33.1	2.4, 33.0	2.5, 28.3	2.5, 33.2	5.1, 80.9	2.6, 80.3	4.0, 69.9	2.4, 33.0
dataset	-11:12; - 10:12; - 12:12	-17:17; -18:18 -10:10	-10:9; -13:13; -18:18	-9:9; 0:22; 0:12	-10:11; -28:28; -11:14	-9:8; -10:11; -9:11	-5:8; -19:18; -21:21	-9:10; -12:13; -15:15	-7:8; -23:23; -16:16
reflns collected	12648	24491	29403	16546	40210	4375	13925	9304	28936
indep reflns	3727	3582	4987	2799	4960	1237	3710	3831	3287
R _{int}	0.026	0.063	0.037	0.123	0.031	0.062	0.076	0.117	0.036
obsd reflns	3189	2373	3554	2363	4518	1076	3087	2108	2692
params	194	194	332	210	243	114	311	359	166
R ₁ (obsd) ^b	0.033	0.049	0.042	0.083	0.032	0.053	0.052	0.061	0.037
wR ₂ (all data) ^c	0.093	0.133	0.111	0.237	0.088	0.161	0.144	0.165	0.101
S ^d	1.07	1.04	1.04	1.02	1.04	1.09	1.09	0.90	1.05
res density [e Å ⁻³]	-0.28, 0.48	-0.45, 0.47	-0.26, 0.26	-0.52, 0.79	-0.64, 0.54	-0.54, 0.42	-0.29, 0.40	-0.41, 0.46	-0.27, 0.47
solution	SHELXTL	SHELXTL	SHELXTL	SHELXTL	SHELXTL	SHELXTL	SHELXTL	SHELXTL	SHELXTL

^a See Methods for complete description of General Procedures for X-ray crystallographic data collection. ^b $R_1 = \sum |F_o| - |F_c| / \sum |F_o|$. ^c $wR_2 = \{\sum [w(F_o^2 - F_c^2)]^2 / \sum [w(F_o^2)]\}^{1/2}$; $w = [\sigma_e^2(F_o^2) + (\chi P)^2 + \gamma P]^{-1}$ and $P = (F_o^2 + 2F_c^2) / 3$; ^d $S = \text{GOF} = \{\sum [w(F_o^2 - F_c^2)]^2 / (n - p)\}^{1/2}$ (n = number of reflections; p = number of parameter)

Mass spectrometry

Compound **2** and its hydrate shows up at 226.1177 m/z by MALDI analysis, which corresponds to the M+2H ion. For all salts tested, the TAABT cation shows up at 225.2 m/z by ESI+. The counterions all appear where expected by ESI-: NO₃⁻ at 62.1 m/z, ClO₄⁻ at 99.1 m/z, 5-nitrimino-1,2,3,4-tetrazolate at 129.1 m/z, and 5-nitro-1,2,3,4-tetrazole at 114.1 m/z.

Nuclear Magnetic Resonance Spectroscopy

Multinuclear NMR spectroscopy (¹H, ¹³C) was used to characterize all compounds. Compound **1** possesses a singlet at 5.15 ppm corresponding to the resonance of the *N*-amine protons, and a singlet at 5.03 ppm corresponding to the *C*-amine proton resonance.⁴⁷ Once azo coupled, a similar spectrum was seen for compounds **2-7**, with the exception of salts **3** and **7** where more powerful acids were used to make the salt (conc. nitric and 5-nitro-1,2,3,4-tetrazole), which caused the peak corresponding to the resonance of *N*-amines protons to broaden due to protic interactions with the solvent. The ¹³C spectrum of **2** shows two peaks corresponding to the *C*-amine carbons and the azo carbon separated by ~1ppm. The ¹³C spectrum of **3** shows a narrowing of these peaks and, for **4**, **5**, and **7**, a complete overlap is observed. This indicates that the chemical environment of the carbons is becoming close to identical as a result of forming an ionic salt.

Infrared Spectroscopy

TAABT (**2**) and its salts, being a symmetrically substituted trans azo complex, is predicted to have IR forbidden N=N stretching vibrations typically seen at 1580-1400 cm⁻¹. The secondary amines of **2** displayed a weak doublet band at 3289.78, and 3111.19 cm⁻¹. Protonation resulted in the appearance of an additional band in this region of 3500-2400cm⁻¹. Broadening of this region was observed for **6•H₂O** and **7** due to the presence of 5-nitrimino-1,2,3,4-tetrazolate and 5-nitro-1,2,3,4-tetrazolate respectively. Deformation bands can be observed for all compounds in the region of 1660-1500 cm⁻¹ for the primary amines and in the region of 1660-1590 cm⁻¹ for the amine salts. Compounds **2** and **3** show strong bands in this region, while **4** and **7** show the formation of shoulder bands in this region possibly due to the N-H⁺ bonds. A strong band was present at ~1310 cm⁻¹ for salts **3**, **4**, **6•H₂O**, and **7** due to the presence of nitrate.⁴⁸

Thermal Stabilities

The thermal behaviors of compounds **2**, **2•H₂O**, **3**, **4**, **5**, **6•H₂O**, and **7** were investigated by combination differential scanning calorimetry – thermogravimetric analysis (DSC/TGA). All measurements were conducted with a heating rate of 10 K·min⁻¹. Decomposition temperatures for **2•H₂O** and **2** were both near 300 °C, while the remaining compounds decomposed below 250 °C. The waters of hydration for **2•H₂O** and energetic salts were lost prior to decomposition. Temperatures of decomposition were determined from the onset of the exothermic detonation peak as seen on the DSC. Onset of decomposition was based on deviation from the baseline and not peak values which can overestimate thermal stabilities. This demonstrates a high degree of thermal stability beyond conventional energetics of similar performance.

Sensitivities

For initial safety testing, the impact and friction sensitivity tests of the prepared nitrogen-rich salts were carried out.^{49,50} The impact sensitivity tests were carried out according to STANAG 4489 (Table 3) and were modified according to instruction using a OZM-BFH-10 drophammer setup.⁵⁰⁻⁵² The friction sensitivity tests were carried out according to STANAG 4487 (Table 3) and were modified according to instruction using a BAM friction tester. Impact sensitivities >40 J and friction sensitivities >360N were considered insensitive.⁵³⁻⁵⁵ Due to the dark orange-red colours of TAABT and energetic salts, determination of decomposition was dependent on whether an audible snap was heard or if a noticeable smell was produced. Compounds **2•H₂O**, **2**, **6•H₂O**, and **7** showed no signs of decomposition over 7 trials of 40 J drop hammer testing and are therefore considered insensitive to impact. Compounds **2**, and **6•H₂O** compressed to a black metallic like material without noticeable decomposition. Salts **3** and **4** show the opposite degree of sensitivity and detonated readily with 1 J impact. Although both **3** and **4** utilize a NO₃⁻ anion, **3** shows a much higher handling sensitivity than **4**. Compounds **2**, **4**, **6•H₂O**, and **7** showed no obvious signs of decomposition after 7 replicate trials at 360 N, indicating the materials are insensitive to friction. Salt **3** also did not produce a smell or audible sign of decomposition, however, **3** is light-orange and showed obvious darkening in the region of 64-80 N. Salts **5** and **7** produced audible snaps at 128 N and 116 N respectively and are therefore considered sensitive to friction.

Energetic Properties

Theoretical predictions of heats of formation and crystalline density were performed using the Gaussian09 program package.⁵⁸ For neutral molecules, these were calculated using the methods of Byrd and Rice, where the molecules were initially optimized using the spin-restricted B3LYP density functional theory with the 6-31G** basis set.⁵⁹⁻⁶⁸ Subsequently the energy of formation was obtained using the electronic energies from the B3LYP/6-311++G(2df,2p) and electrostatic parameters on the 0.001 electron/bohr³ isosurface. For ionic species, the structures were optimized in a similar manner to the neutral species, while the heats of formation were obtained from the G3MP2(B3LYP) energies and either the Gutowski for 1:1 salts or Jenkins derived (for all other salts) lattice enthalpies.⁶⁹⁻⁷³ Performance values were calculated from theoretical heats of formation, and when available, experimental room temperature crystal densities (otherwise calculated densities were used) using the EXPLO6.05 software. The density that was used for EXPLO6.05 calculations was outlined in each column. Performance is calculated from the input of the molecular formula, calculated heats of formation, and the maximum densities according to their crystal structures at low temperatures or calculated densities in cases where experimental values are not obtained. EXPLO6.05 is based on the chemical equilibrium, steady state model of detonation. It uses Cowan–Fickett's equation of state for solid carbon and Becker–Kistiakowsky–Wilson's equation of state (BKW EOS) for gaseous detonation products. Compound **2**, in addition to salts **3-7**, all showed high thermal stability, and high performance with


detonation pressures of ~26-30 GPa and detonation velocities comparable in performance to RDX.

Table 3. Energetic performance of TAABT and energetic salts


Entry	2•H ₂ O	2	3	4	5	6•H ₂ O	7	RDX
Formula	C ₄ H ₈ N ₁₂ •H ₂ O	C ₄ H ₈ N ₁₂	[C ₄ H ₁₀ N ₁₂] ²⁺ [2(NO ₃)] ²⁻	[C ₄ H ₉ N ₁₂] ⁺ [NO ₃] ⁻	[C ₄ H ₉ N ₁₂] ⁺ [ClO ₄] ⁻	[C ₄ H ₉ N ₁₂] ⁺ [CHN ₆ O ₂] ⁻ •(H ₂ O)	[C ₄ H ₁₀ N ₁₂] ²⁺ [2(CN ₅ O)] ²⁻	C ₃ H ₆ N ₆ O ₆
FW/g mol ⁻¹	242.20	224.19	350.21	287.20	324.64	372.27	454.29	222.12
IS ^a /J	>40	>40	<1	>40	<1	>40	>40	7.5
FS ^b /N	>360	>360	64-80	>360	128	>360	116	120
N ^c /%	69.40	74.97	63.40	55.99	51.77	67.73	67.83	37.84
Ω ^d /%	-79.27	-85.64	-31.98	-52.92	-41.89	-64.47	-45.79	-21.61
T _{Dec} ^e /°C	291	302	224	230	254	220	241	205 ⁵⁶
ρ _{xray} ^f /g cm ⁻³	-	-	1.740	-	-	-	1.703	-
ρ _{xray} ^g /g cm ⁻³	-	-	1.776	-	1.821	-	1.762	1.858 ⁵⁷
ρ _{calc} ^h /g cm ⁻³	1.594	1.683	1.827	1.711	1.791	1.714	1.767	-
*EXPLO6.05 ³⁸								
-Δ _{ex} U ^o /kJkg ⁻¹	-	3896	-4220	-4480	-5115	-4320	-4408	5740
T _{Det} ⁱ /K	-	2576	3003	3004	3582	2909	3189	3745
P _{CJ} ^k /GPa	-	26.9	27.4	27.3	29.8	27.8	25.6	33.6
V _{Det} ^k /m s ⁻¹	-	8742	8444	8585	8584	8742	8340	8801
V _o ^m /L kg ⁻¹	-	818	858	857	824	865	829	784

Entry	2•H ₂ O a	2•H ₂ O b
Formula	C ₄ H ₈ N ₁₂ •H ₂ O	C ₄ H ₈ N ₁₂ •H ₂ O
ρ _{xray} ^f /g cm ⁻³	-	1.703
ρ _{xray} ^g /g cm ⁻³	1.626	1.723
-Δ _{ex} U ^o /kJkg ⁻¹	-3637	-3621
T _{Det} ⁱ /K	2443	2400
P _{CJ} ^k /GPa	24.3	27.3
V _{Det} ^k /m s ⁻¹	8416	8839
V _o ^m /L kg ⁻¹	862	857

STANAG 4487
BAM Friction Tester



STANAG 4489
BAM Drop Hammer



^a Impact sensitivity (BAM drop hammer 1 of 6). ^b Friction sensitivity (BAM friction tester 1 of 6). ^c Percent nitrogen ^d Oxygen balance (Ω = 1600/MW(2xC+0.5yH-zO)). ^e Temperature of decomposition. ^f Density single crystal x-ray crystal diffraction at room temperature. ^g Density single crystal x-ray crystal diffraction at 150 K. ^h Computationally predicted density. ⁱ Enthalpy of Explosion. ^j Temperature of detonation. ^k Detonation pressure according to Chapman–Jouguet. ^l Velocity of detonation. ^m Volume of detonation gases. *EXPLO5 values calculated using experimentally obtained room temperature densities when available, otherwise, values calculated using calculated using computationally predicted densities. The density values outline in a box were used for EXPLO5 calculations.

Compound **2•H₂O b** shows the highest detonation velocity of all materials tested at 8839 m s⁻¹, which exceeds RDX. Interestingly, this material shows a higher density and performance than anhydrous **2**, which may indicate that the actual density for anhydrous **2** may be higher than the calculated density and the performance is therefore higher than what is reported in Table 3. Compound **2** and its hydrate both show extremely high thermal stability with thermal onsets for decomposition at >300 °C, friction sensitivities >360 N, and impact sensitivities >40 J. This makes **2** a very promising thermally stable IHE alternative to RDX. The energetic salts produced have a higher density and have slightly improved detonation pressures, but with the trade-off for higher sensitivity.

Conclusions

The skillset of the synthetic chemist must grow to meet the demand for novel energetics and increasingly complex heterocyclic

materials. Electrochemistry allows the modern chemist to broaden their synthetic toolbox while mitigating the waste streams produced from traditional synthesis. This work has demonstrated electrochemistry's utility to the synthetic energetic materials chemist with the facile production of high-performance energetic materials through electrochemical synthesis in mild environment with low-hazard waste streams. All materials produced in this work demonstrate high detonation performances that rival RDX, and remarkably low thermal, impact, and friction sensitivities. These unique materials would be difficult, if not impossible, to obtain through conventional synthesis techniques due to the presence of the highly reactive *N*-amine or guanazine. Further exploration into the electrochemical formation of reactive *N*-nitrene species could produce a variety of interesting novel high nitrogen content heterocycles for use in energetics, medicine, and biology that may not be available by other means.⁷⁴

Acknowledgements

The authors want to thank lab members Matthew Gettings, Doinique Wozniak, and Shannon Creegan for their support in the lab. Financial support of our lab is provided by the Office of Naval Research under grant N00014-19-1-2089, the Army Research Office (ARO) under grant number W911NF-18-1-0463 and by Purdue University. The National Science Foundation is acknowledged for funding through the Major Research Instrumentation Program under Grant No. CHE 1625543 for the single crystal X-ray diffractometer.

Author Information

Corresponding Author

*E-mail: dpiercey@purdue.edu

Notes

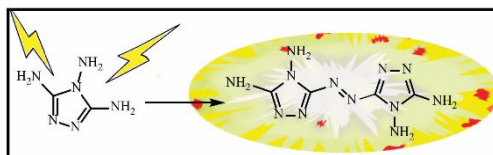
The authors declare no competing financial interest.

References

- D. G. Piercey, D. E. Chavez, B. L. Scott, G. H. Imler, D. A. Parrish. *Angew. Chem. Int. Ed.* 2016, **55** (49), 15315–15318.
- G. Zhao, C. He, P. Yin, G. H. Imler, A. A. Parrish, J. N. M. Shreeve. *J. Am. Chem. Soc.* 2018, **140** (10), 3560–3563.
- C. Sun, C. Zhang, C. Jiang, C. Yang, Y. Du, Y. Zhao, B. Hu, Z. Zheng, K. O. Christe. *Nat Commun.* 2018, **9**, 1269.
- L. Hu, P. Yin, G. Zhao, C. He, G. H. Imler, D. A. Parrish, H. Gao, J. N. M. Shreeve. *J. Am. Chem. Soc.* 2018, **140** (44), 15001–15007.
- T. M. Klapötke, C. Petermayer, D. G. Piercey, J. Stierstorfer. *J. Am. Chem. Soc.* 2012, **134** (51), 20827–20836.
- M. Reichel, M. Dosch, T. M. Klapötke, K. Karaghiosoff. *J. Am. Chem. Soc.* 2019, **141** (50), 19911–19916.
- W. L. Yuan, G. H. Tao, L. Zhang, Z. Zhang, Y. Xue, L. He, J. Huang, W. Yu. *Sci Rep.* 2020, **10**, 4477.
- M. Deng, Y. Feng, W. Zhang, X. Qi, Q. Zhang. *Nat. Commun.* 2019, **10**, 1339.
- P. F. Pagoria, G. S. Lee, A. R. Mitchell, R. D. Schmidt. *Thermochimica Acta.* 2002, **384** (1-2), 187.
- H. Gao, J. N. M. Shreeve. *Chem. Rev.* 2011, **111** (11), 7377.
- P. Leffler, E. Brännäs, D. Ragnvaldsson, H. Wingfors, R. J. Berglund. *Tox. Environ. Health, Part A.* 2014, **77** (19), 1183.
- F. Testud, J. M. Glandau, J. Descotes. *J. Toxic. Clin Toxic.* 1996, **34** (1), 109.
- P. Y. Robidoux, C. Svendsen, M. Sarrazin, S. Thiboutot, G. Ampleman, J. Hawari, J. M. Weeks, G. I. Sunahara. *Arch. Environ. Cont. Tox.* 2004, **48** (1), 56.
- P. E. Eaton, M. X. Zhang, R. Gilardi, N. Gelber, S. Iyer, R. Surapaneni. *Propellants, Explosives, Pyrotechnics.* 2002, **27** (1), 1.
- D. P. Deeter, J. C. Gaydos. *Occupational health: the soldier and the industrial base.* Office of the Surgeon General, U.S. Dept. of the Army, Falls Church, VA, 1993.
- V. Thottempudi, H. Gao, J. N. M. Shreeve. *J. Am. Chem. Soc.* 2011, **133** (16), 6464.
- H. Lund, O. Hammerich. *Organic electrochemistry.* New York: Marcel Dekker, 2001.
- E. J. Horn, B. R. Rosen, P. S. Baran. *ACS Cent. Sci.* 2016, **2** (5), 302–308.
- M. Yan, Y. Kawamata, P. S. Baran. *Chem. Rev.* 2017, **117** (21), 13230–13319.
- J. Grimshaw, *Electrochemical Reactions and Mechanisms in Organic Chemistry*, Elsevier, 2000.
- Y. Yuan, A. Lei. *Nat Commun.* 2020, **11**, 802.
- J. Volke, F. Liška, *Electrochemistry in Organic Synthesis.* Springer-Verlag, Berlin Heidelberg, 1994.
- C. A. C. Sequeira, D. M. F. J. Santos. *Braz. Chem. Soc.* 2009, **20** (3), 387.
- M. P. Cronin, A. I. Day, L. Wallace. *J. Haz. Mater.* 2007, **149** (2), 527.
- L. Wallace, C. J. Underwood, A. I. Day, D. P. Buck. *New J. Chem.* 2011, **35** (12), 2894.
- D. W. Firsich, *An electrochemical preparation of hexanitrostilbene (HNS) from hexanitrobibenzyl (HNBB).* (Final Report. OSTI identifier 5043970, 1986).
- Paraskos, M. Hawkins, T. Lister, R. Fox, P. Symons. *Final Report: Pilot-Scale Electro-chemical Synthesis of Potassium 2,2-dinitroethanate.* (SERDP project report WP-1460, 2011).
- K. Majumdar, K. Ray. *Synthesis.* 2011, **23**, 3767.
- Z. Ye, F. Wang, Y. Li, F. Zhang. *Green Chem.* 2018, **20** (23), 5271.
- P. Xu, H. C. Xu. *ChemElectroChem.* 2019, **6** (16), 4177.
- Y. Li, Z. Ye, N. Chen, Z. Chen, F. Zhang. *Green Chem.* 2019, **21** (15), 4035.
- H. He, J. Du, B. Wu, X. Duan, Y. Zhou, G. Ke, T. Huo, Q. Ren, L. Bian, F. Dong. *Green Chem.* 2018, **20**, 3722–3726.
- X. Fu, J. Du, B. Wu, G. Ke, J. Wang, Y. Zhou, K. Liu, Y. Yang, Q. Yang, B. Xiong, H. He. *J. Electrochem. Soc.* 2020, **167**, 065503.
- L. Chen, L. M. Barton, J. C. Vantourout, Y. Xu, C. Chu, E. C. Johnson, J. J. Sabatini, P. S. Baran. *Org. Process Res. Dev.* 2020, In Press, <https://doi.org/10.1021/acs.oprd.0c00270>
- L. Türker. *Def. Tech.* 2016, **12** (1), 1.
- R. G. Child. *J. Heterocycl. Chem.* 1965, **2**, 98.
- C. Li, C. Deng, B. Zhao, M. Wang, M. Zhang, Z. Zhou. *Propellants, Explosives, Pyrotechnics.* 2020, **45** (4), 531–535.
- M. Suceška, EXPLO6.05 program, Zagreb, Croatia, 2010.
- T. Siu, C. J. Picard, A. K. Yudin. *J. Org. Chem.* 2005, **70** (3), 932.
- C. G. Savarin, C. Grisé, J. A. Murry, R. A. Reamer, D. L. Hughes. *Org. Lett.* 2007, **9** (6), 981.
- K. Yudin, *Aziridines and Epoxides in Organic Synthesis.* (Wiley-VCH Verlag GmbH & Co, 2007).
- D. Kvaskoff, P. Bednarek, L. George, K. Waich, C. Wentrup. *J. Org. Chem.* 2006, **71** (11), 4049.
- J. Bard, L. R. Faulkner, *Electrochemical methods: fundamentals and applications Ch 12.* (John Wiley, New York, 2, 2002).
- T. M. Klapötke, D. G. Piercey, J. Stierstorfer. *Dalton Trans.* 2012, **41** (31), 9451.
- D. Wozniak, D. G. Piercey, M. Zeller, E. F. C. Byrd. *ChemOpen.* 2019 DOI: 10.1002/open.202000053.
- N. Dubouis, A. Grimaud. *Chem. Sci.* 2019, **10**, 9165.
- C. Darwich, T. M. Klapötke, J. Welch, M. Suceška. *Propellants, Explos., Pyrotech.* 2007, **32**, 235.
- Larkin, P. *Infrared and Raman Spectroscopy Principles and Spectral Interpretation Ch.7.* (Elsevier, 2011).
- M. Suceška. *Test Methods for Explosives.* Springer Science & Business Media. 2012.
- BAM FALL HAMMER BFH-12A. Can be found under: <http://www.ozm.cz/en/sensitivity-tests/bam-fall-hammer-bfh-12a/>. 2020.

51. NATO standardization agreement (STANAG) on explosives, impact sensitivity tests, no. 4489, 1, 1999.
52. WIWEB-Standardarbeitsanweisung 4–5.1.02, Ermittlung der Explosionsgefährlichkeit, hier der Schlagempfindlichkeit mit dem Fallhammer, 2002.
53. NATO standardization agreement (STANAG) on explosives, friction sensitivity tests, no. 4487, 1, 2002.
54. WIWEB-Standardarbeitsanweisung 4–5.1.03, Ermittlung der Explosionsgefährlichkeit oder der Reibeempfindlichkeit mit dem Reibeapparat, 2002.
55. Impact: Insensitive > 40 J, Less Sensitive ≥ 35 J, Sensitive ≥ 4 J, Very Sensitive ≤ 3 J; Friction: Insensitive 360 N, Less Sensitive = 360 N, Sensitive < 360 N and > 80 N, Very Sensitive ≤ 80 N, Extreme Sensitive ≤ 10 N, According to the UN Recommendations on the Transport of Dangerous Goods (+) indicates: not safe for transport.
56. J. P. Agrawal, *High Energy Materials*. (Wiley-VCH, Weinheim, 1, 189, 2010).
57. P. Hakey, W. Ouellette, J. Zubieta, T. Korter, *Acta Crystallogr Sect. E: Struct. Rep. 2008 Online*, **E64**, o1428.
58. M. J. Frisch, M. J. Frisch, G. W. Trucks, H. B. Schlegel, G. E. Scuseria, M. A. Robb, J. R. Cheeseman, G. Scalmani, V. Barone, G. A. Petersson, H. Nakatsuji, X. Li, M. Caricato, A. Marenich, J. Bloino, B. G. Janesko, R. Gomperts, B. Mennucci, H. P. Hratchian, J. V. Ortiz, A. F. Izmaylov, J. L. Sonnenberg, D. Williams-Young, F. Ding, F. Lipparini, F. Egidi, J. Goings, B. Peng, A. Petrone, T. Henderson, D. Ranasinghe, V. G. Zakrzewski, J. Gao, N. Rega, G. Zheng, W. Liang, M. Hada, M. Ehara, K. Toyota, R. Fukuda, J. Hasegawa, M. Ishida, T. Nakajima, Y. Honda, O. Kitao, H. Nakai, T. Vreven, K. Throssell, J. A. Montgomery, Jr., J. E. Peralta, F. Ogliaro, M. Bearpark, J. J. Heyd, E. Brothers, K. N. Kudin, V. N. Staroverov, T. Keith, R. Kobayashi, J. Normand, K. Raghavachari, A. Rendell, J. C. Burant, S. S. Iyengar, J. Tomasi, M. Cossi, J. M. Millam, M. Klene, C. Adamo, R. Cammi, J. W. Ochterski, R. L. Martin, K. Morokuma, O. Farkas, J. B. Foresman, D. J. Fox. Gaussian 09, Revision A.02. Gaussian, Inc., Wallingford CT, 2016.
59. B. M. Rice, J. J. Hare, E. F. C. Byrd. *Phys. Chem. A*. 2007, **111**, 10874-10879.
60. B. M. Rice, & E. F. C. Byrd. *J. Comput. Chem.* 2013, **34**, 2146-2151.
61. E. F. C. Byrd, B. M. Rice. *J. Phys. Chem. A*. 2009, **113**, 345-352.
62. D. Becke. *J. Chem. Phys.* **1993**, **98**, 5648-5652.
63. Lee, W. Yang, R. G. Parr. *Phys. Rev. B*. 1988, **37**, 785
64. S. H. Vosko, L. Wilk, M. Nusair. *Can. J. Phys.* 1980, **58**, 1200–1211.
65. P. J. Stephens, F. J. Devlin, C. F. N. Chabalowski, M. J. Frisch. *J. Phys. Chem.* 1994, **98**, 11623-11627.
66. R. Krishnan, J. S. Binkley, R. Seeger, J. A. People. *J. Chem. Phys.* 1980, **72**, 650-654.
67. M. J. Frisch, J. A. Pople, J. S. Binkley. *J. Chem. Phys.* 1984, **80**, 3265-3269.
68. P. V. R. Schleyer. *et. al. J. Am. Chem. Soc.* 1984, **106**, 6467-6475.
69. G. Baboul, L. A. Curtiss, P. C. Redfern, K. Raghavachari. *J. Chem. Phys.* 1999, **110**, 7650–7657.
70. K. E. Gutowski, R. D. Rogers, D. A. Dixon. *J. Phys. Chem. B*. 2007, **111**(18), 4788-4800.
71. H. D. B. Jenkins, H. K. Roobottom, J. Passmore, L. Glasser. *Inorg. Chem.* 1999, **38**(16), 3609-3620.
72. H. D. B. Jenkins, D. Tudela, L. Glasser. *Inorg. Chem.* 2002, **41**, 2364-2367.
73. H. D. B. Jenkins, L. Glasser. *Inorg. Chem.* 2006, **45**, 1754.
74. R. D. Taylor, M. Maccoss. *A. D. G. Lawson. J. of Med. Chem.* 2014, 57 (14), 5845.
75. T. M. Klapötke, J. Stierstorfer. *Helv. Chimica Acta*. 2007, **90**(11), 2132.
76. T. M. Klapötke, D. G. Piercey, N. Meheta, K. D. Oyler, M. Jorgensen, S. Lenahan, J. S. Salan, J. W. Fronabarger, M. D. Williams. *Zeit. Anorg. Allg. Chem.* 2013, **639** (5), 681-688.
77. Description - ElectraSyn 2.0 Package. Can be found under: <https://www.ika.com/en/Products-Lab-Eq/Electrochemistry-Kit-csp-516/ElectraSyn-20-Package-cpdt-20008980/>
78. J. L. Dempsey. *J. Chem. Educ.* 2017, **95** (2), 197.
79. Bruker. Apex3 v2018.7-2, Saint V8.38A, Bruker AXS Inc.: Madison (WI), USA 2018.
80. L. Krause., R. Herbst-Irmer, G. M. Sheldrick, D. Stalke. *J. Appl. Cryst.* 2015, **48**, 3-10.
81. G. M. Sheldrick. *Acta Crystallogr A*. 2008, **64**(1), 112–122.
82. G. M. Sheldrick. *Acta Crystallogr Sect C Struct. Chem.* 2015, **71**(1), 3–8.

For table of contents only.



Electrochemical azo coupling of guanazine yields novel thermally insensitive high-explosive. DFT and EXPLO 6.05 calculations reveal energetic properties that rival RDX making this a potentially cheap, and green alternative to traditional energetics.